



Small cell lung cancer induces synaptic scaling to alter neuronal excitability



Aiden J. Houcek^{1,2,3}, Burak Uzay^{1,2}, Geena V. Ildefonso^{4,5}, Tolu Omokehinde^{4,5}, Lisa M. Monteggia^{1,2}, Vito Quaranta^{1,4}, Amanda Linkous¹ & Ege T. Kavalali^{1,2}

Tumor cell plasticity in novel microenvironments is central to the integration and subsequent growth of metastatic cells. However, the functional consequences of tumor cell integration with central neurons remains understudied. Here, we address this question using small cell lung cancer (SCLC), which has an extraordinary propensity to metastasize to the brain in humans. Transcriptomic and electrophysiological analysis of SCLC cells in neuronal microenvironments reveal a heterogeneous population of synapse-forming SCLC cells with neurons. While a proportion of neuron-SCLC synapses are blocked by AMPA receptor antagonists, we also find a sensitivity of these synapses to GABA_A receptor inhibition. The functional integration of SCLC with central neurons induced multiplicative synaptic upscaling between neurons and dysregulated neuronal excitability. Aberrant excitation in human neurons with SCLC was sustained by synaptic NMDA receptor activation and can be reduced by the FDA approved NMDA receptor blocker memantine. These findings reveal strategies to normalize tumor-induced exacerbation of aberrant neuronal activity.

Brain metastasis drastically constrains treatment options and negatively affects the quality of life in cancer patients. Studies attempting to prevent or control brain metastasis have largely focused on cancer cell affinity for cerebral tissue, or tumor growth-promoting factors in the brain^{1,2}. Less understood are the biological bases for the neurological symptoms experienced by brain metastasis patients, which include seizures, headaches, changes in cognitive function, motor deficits, and personality changes, amongst others³. While brain tissue inflammation, compression and edema undoubtedly contribute to these symptoms, we set out to explore the possibility that cancer cells may alter the neuronal microenvironment in specific ways.

To this end, we focus on small cell lung cancer (SCLC), which has an extraordinary propensity to metastasize to the brain^{4,5}, to the point that SCLC patients, whether or not presenting with brain metastasis, are prescribed prophylactic brain irradiation. The propensity for SCLC cells to metastasize to the brain may arise from several underlying characteristics of these neoplastic cells. In their non-neoplastic counterpart, neuroendocrine cells in the lung receive synaptic input from the nodose, dorsal root, and jugular ganglia⁶. Furthermore, anatomical features such as access to vasculature in the lung is suggested to contribute to metastasis from this organ. Current drug treatments for patients with SCLC include platinum-based chemotherapeutics and etoposide⁷. However, specialized treatments for SCLC brain metastasis remain poorly understood and developed. Seizures

are also a common symptom of brain metastasis, although the underlying mechanisms of tumor-induced augmentation of neural excitability remain largely unknown. Previous work has revealed that glioma cells can form functional synaptic contacts with neurons and alter the excitability of both proximal and distal neurons⁸⁻¹¹. These insights into the functional integration of primary brain tumors represent an untapped avenue of research and therapeutic opportunities potentially applicable to both primary and secondary brain metastasis. Recent work studying SCLC integration with neurons has also revealed evidence of neuronal synapse formation on SCLC cells^{12,13}. However, the underlying mechanisms governing SCLC-induced changes in neuron function that lead to the neurological abnormalities associated with brain metastasis remain poorly understood.

Here we show that SCLC cells can form functional synapses with neurons. Synapse-forming SCLC cells revealed a heterogeneous sensitivity to the AMPA receptor antagonist cyanquinaline (CNQX) and were also reduced following GABA_A receptor blockade. The functional integration of SCLC cells dysregulated spontaneous firing properties and induced multiplicative synaptic upscaling between induced human neurons. Aberrant firing activity between human neurons with SCLC cells can be rapidly normalized using NMDA receptor antagonists. Together, these findings illustrate how the functional integration of SCLC cells drives dysregulated communication between neurons and potential therapeutic strategies to alleviate neurological abnormalities in SCLC brain metastasis.

¹Department of Pharmacology, Vanderbilt University, Nashville, TN, USA. ²Vanderbilt Brain Institute, Vanderbilt University, Nashville, TN, USA. ³Department of Biological Sciences, Vanderbilt University, Nashville, TN, USA. ⁴Department of Biochemistry, Vanderbilt University, Nashville, TN, USA. ⁵These authors contributed equally: Geena V. Ildefonso, Tolu Omokehinde. e-mail: ege.kavalali@vanderbilt.edu

Results

Functional neuron-to-SCLC synapses

We first asked if SCLC cells form functional synaptic contacts with neurons. To address this question, we added H69 (SCLC-A neuroendocrine subtype) or H841 (SCLC-Y non-neuroendocrine) cells to rat hippocampal neurons 10–14 days and assessed the synaptic integration of SCLC cells with neurons 10–14 days

later using whole cell patch-clamp electrophysiology. We identified SCLC cells in vitro using mKate2 fluorescence (Fig. 1A) and detected evoked and spontaneous currents on SCLC cells (Fig. 1B–F) using a bipolar stimulating electrode immersed in the external bath solution. The currents on SCLC cells facilitated upon 20 Hz stimulation in contrast to the robust synaptic depression of isolated evoked postsynaptic currents between neurons

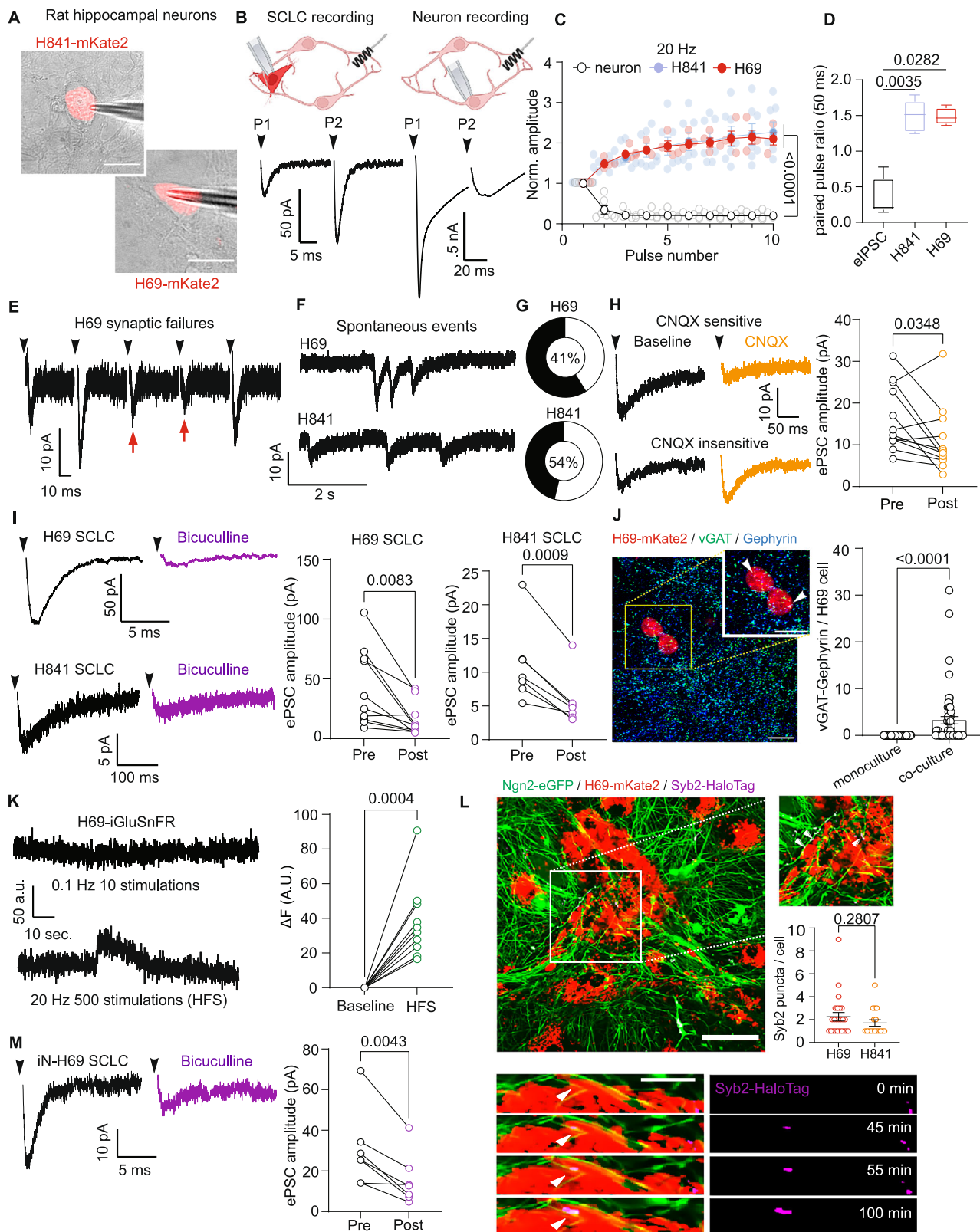


Fig. 1 | A minor subset of SCLC cells form functional synapses with central neurons. A Fluorescent and bright field merged images of SCLC cells expressing mKate2 in co-culture with hippocampal neurons. Scale bar = 40 μ m. B ePSCs on H69 cells and neuronal eIPSCs in response to first two pulses at a 50 ms interstimulus interval (ISI). C Normalized amplitudes and D paired-pulse ratios of ePSCs on SCLC cells and neuronal eIPSCs at 50 ms ISI. PPRs presented in (D) are P2/P1 from stimulus train in (C) ($n = 6$ neurons, 4 H69, and 7 H841 cells). (E,F) Example traces of evoked failures and spontaneous synaptic currents on SCLC cells. G Quantification of percent of total SCLC cells with detectable evoked and spontaneous PSCs. H Example traces and quantification of ePSC amplitudes on H69 cells before and after application of 100 μ M CNQX ($n = 12$ cells). I Example traces and quantification of ePSC amplitudes on H69 and H841 cells before and after application of 100 μ M bicuculline ($n = 10$ H69 cells and seven H841 cells). J Example

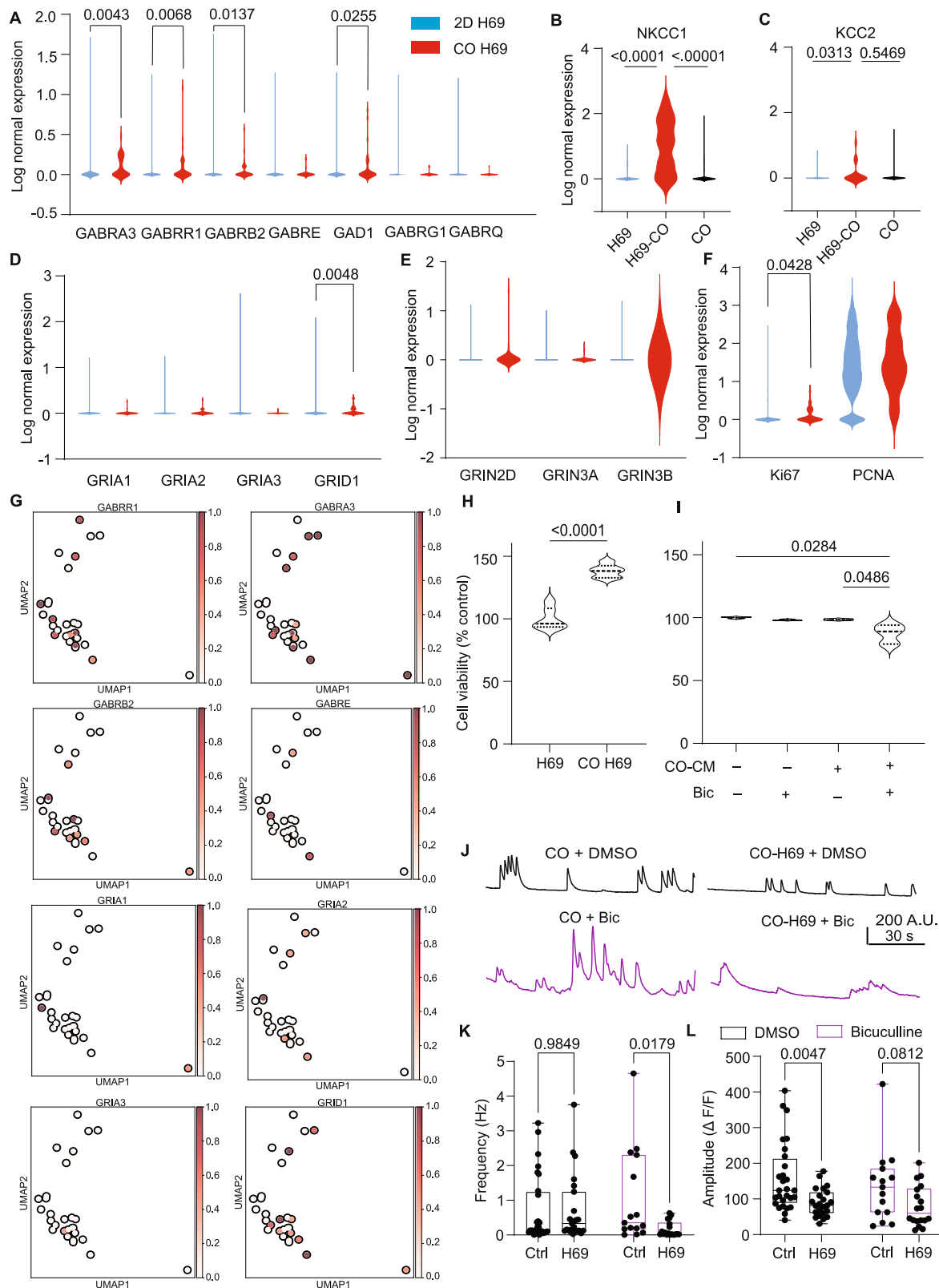
image and quantification of GABAergic synapse markers vGAT and Gephyrin on H69 monocultures ($n = 65$ H69 cells) and H69 cells with rat hippocampal neurons ($n = 58$ H69 cells). Scale bar = 20 μ m. K Example trace of H69 SCLC iGluSnFR fluorescence in response to low or high frequency stimulation and quantification of H69 fluorescence intensity following HFS ($n = 10$ cells). L Example images of SCLC cells with iNs expressing Syb2-HaloTag and quantification of Syb2 puncta per SCLC cell. Scale bar = 50 μ m and 5 μ m for bottom panels ($n = 24$ H69 and 17 H841 cells from 5 fields of view). M Example trace and quantification of ePSC amplitudes on H69 cells in iN cultures before and after application of 100 μ M bicuculline ($n = 7$ cells). All summary graphs show mean \pm SEM. Statistical significance was assessed by two-way ANOVA with Dunnett's multiple comparisons (C); one-way ANOVA with Dunn's multiple comparisons (D); paired-samples t-test (H,I,K,M); independent samples t-test (J,L).

(Fig. 1C, D). In support of these facilitating currents on SCLC being mediated by presynaptic neurons, we observed evidence of synaptic failures upon repetitive stimulation and spontaneous events (Fig. 1E, F). Altogether, we detected evoked currents in approximately 40% of the total SCLC cells we recorded from (Fig. 1G). Interestingly, perfusing the AMPAR antagonist CNQX revealed populations of CNQX-sensitive and insensitive tumor cells (Fig. 1H), whereas application of the competitive GABA_A receptor antagonist bicuculline consistently reduced evoked currents on SCLC cells (Fig. 1I). Immunostaining for GABAergic synapse markers on H69 SCLC supported this pharmacological evidence that SCLC cells can form functional GABAergic synapses with neurons (Fig. 1J). We sought to further explore this variability of neuron-SCLC synapses to AMPAR antagonists by selectively expressing the optical glutamate sensor iGluSnFR in H69 cells and measuring changes in fluorescence in response to single or high-frequency stimulation of the surrounding network. Low-frequency stimulations at 0.1 Hz did not produce peaks in iGluSnFR fluorescence, while repetitive stimulation at 20 Hz did result in an increase in H69 iGluSnFR fluorescence (Fig. 1K), indicating that H69 cells are subjected to released glutamate from neurons. We then utilized induced human neurons (iNs) derived from human embryonic stem cells (hESCs), which almost exclusively form glutamatergic synapses following rapid single-step induction using neurogenin-2 to further explore the functional integration of SCLC with neurons^{14–16}. We co-cultured SCLC cells with iNs from days 20–25 and measured the functional integration of SCLC cells 2–3 weeks later, when iNs were functionally mature at approximately 45 days of age. We first visualized synapse formation on SCLC in this system, utilizing a presynaptic synaptobrevin2 – HaloTag. This probe was co-transduced with Ngn2-eGFP vectors in hESCs, which allowed us to selectively visualize presynaptic terminals colocalized to eGFP in iNs following acute incubation of iN-SCLC co-cultures with a HaloTag ligand. Live imaging at 24 hours and 12 days of incubation with SCLC revealed dynamic synapse formation and elimination on SCLC cells (Fig. 1L). Whole-cell voltage clamp recordings of evoked activity on H69 SCLC with iNs revealed a similar form of short-term facilitation that was detected on SCLC with rat hippocampal neurons (Supplementary Fig. 1A–D). These events were also detected on H841 with iNs, but not detected in monocultures of either SCLC cell line (Supplementary Fig. 1E). Evoked currents on H69 with iNs were also not robustly reduced following perfusion of 100 μ M CNQX or GYKI 53655, an AMPAR antagonist that acts on transmembrane anchoring receptor proteins^{17,18} (Supplementary Fig. 1F). This failure of CNQX and GYKI to consistently reduce evoked amplitudes on H69 cells was in stark contrast to the robust reduction of eEPSCs between iNs following CNQX or GYKI perfusion, indicating that these drugs are effective in blocking AMPAR-mediated synaptic transmission (Supplementary Fig. 1G). Given these data and our previous findings that SCLC cells preferentially form GABAergic synapses with rat hippocampal neurons, we asked if bicuculline also reduces ePSCs on SCLC in iN cultures. Indeed, perfusion of 100 μ M bicuculline resulted in a significant reduction of ePSCs on H69 cells (Fig. 1M). In support of this finding, these bicuculline-sensitive currents on H69 SCLC could also be produced by perfusing the GABA_A receptor agonist muscimol (Supplementary Fig. 1H). Interestingly, depolarization of H69 SCLC cells generated

activity resembling spiking, which was not detected in H841 cells (Supplementary Fig. 1I). To further confirm that these currents on H69 cells are mediated by synaptic transmission, we measured vesicle fusion on H69 cells in the absence of electrical stimulation of the surrounding network using hypertonic sucrose, which triggers fusion of synaptic vesicles in the readily releasable pool (RRP) independent of calcium influx^{19,20}. Here, we detected vesicle fusion on H69 in approximately 30% of the total number of recorded cells (Supplementary Fig. 1J). Of note, these events were not tightly coupled to perfusion of hypertonic sucrose and often detected up to 1 min following sucrose application. Still, these events were also detected in the presence of CNQX and resemble classical features of bona fide synaptic currents with a fast asymmetric deflection from the baseline in the absence of any stimulation artifacts (Supplementary Fig. 1K). Tumor cell RRP sizes were significantly smaller than neuronal RRP sizes (Supplementary Fig. 1L), consistent with relatively high PPR values and short-term facilitation observed on these tumor cells. Altogether, these findings suggest that a minor subset of SCLC cells can form functional glutamatergic and GABAergic synapses with central neurons, even in largely excitatory populations of induced human neurons²¹.

SCLC in cerebral organoids

Current model systems for SCLC frequently lack a realistic human tumor microenvironment and, thus, rarely exhibit the destructive colonization of distant organ sites that is routinely observed in SCLC patients with brain metastasis. Using hESC-derived cerebral organoids (COs), we have previously shown that the CO microenvironment maintains the invasive phenotype and intratumoral heterogeneity of tumors that grow within the human brain^{22–24}. Thus, to assess adaptive molecular changes of H69 SCLC cells when grown in a human brain microenvironment, we seeded tumor cells in COs and conducted single-cell RNA sequencing (scRNA-seq) of H69 cells (Supplementary Fig. 2A, B). Differential expression profiles of H69 cells in COs were compared to H69 grown as 2D monocultures. H69 cells were seeded at a density of 100,000 cells per organoid and collected for scRNA-seq after 48 h of incubation. Concordant with our electrophysiological analysis, we found that H69 cells increased the expression of genes related to postsynaptic GABA_A receptors when grown within COs (Fig. 2A). The chloride transporter NKCC1 was also robustly upregulated in H69 cells grown in COs whereas NKCC2 was modestly elevated in H69 cells in COs, indicating SCLC cells establish high intracellular chloride gradients in neuronal environments (Fig. 2B, C). Analysis of gene transcripts related to AMPA and NMDA receptors remain largely unchanged between 2D H69 cells and those in COs, with the exception of GRID1 (Fig. 2D, E). We found an increase in the proliferation marker Ki67 in H69 grown with COs relative to H69 monocultures, whereas PCNA expression was not changed between these conditions (Fig. 2F). Further analysis of GABA_A and glutamate receptor subunit expression in individual H69 cells within COs revealed a high degree of heterogeneity in postsynaptic gene expression levels, with some tumor cells robustly upregulating postsynaptic gene transcripts relative to the minor or absent changes in other H69 tumor cells (Fig. 2G). While more tumor cells showed a bias towards GABAergic subunit expression, several tumor cells also increased expression of AMPA and NMDAR



subunits within COs (Fig. 2G and Supplementary Fig. 2C), consistent with the variable sensitivity of these tumor cells to CNQX. Analysis of metabotropic GABA receptors revealed a decrease in GABA_B receptor subunit expression in H69 with COs (Supplementary Fig. 2D). Morphologically, we observed structures resembling tumor microtubes in H69 SCLC cells grown with COs (Supplementary Fig. 2E), similar to previous observations of

glioma tumor microtube formation in COs²² and an increase in cell viability when H69 cells were grown with COs (Fig. 2H), consistent with our transcriptomic analysis of the proliferative marker Ki67. When we measured cell viability of H69 tumor organoids grown in fresh or conditioned media from COs, we found bicuculline treatment reduced tumor cell viability when grown in conditioned media from COs (CO-CM) whereas bicuculline had

Fig. 2 | H69 SCLC undergoes heterogeneous transcriptomic changes in cerebral organoids and induces a bicuculline sensitivity. A Quantification of log normal GABA receptor subunit expression in H69 monoculture or in COs. B,C Expression levels of chloride transporters NKCC1 and KCC2 in H69 SCLC relative to CO cells. D,E Quantification of AMPA and NMDA subunit expression in H69 monocultures relative to H69 in COs. F Quantification of proliferative markers Ki67 and PCNA in H69 monoculture or in COs. G UMAP plots of H69 cells in COs for synapse-related genes. Each UMAP plot shows the same H69 cells with different genes of interest. H Quantification of cell viability using alamarBlue assay of H69 relative to H69 grown with COs ($n = 6$ wells per condition). I Quantification of H69 cell viability in

CO-conditioned media with bicuculline treatment ($n = 3$ wells per condition). J Example recordings of spontaneous calcium transients in cerebral organoids. K,L Quantification of frequency and amplitude of spontaneous events in fields of view in COs with SCLC and treated with bicuculline for 72 h. Significance was assessed using Wilcoxon signed-rank test (A–F); two-way ANOVA with Sidak's (K and L) or Tukey's (I) multiple comparisons test; independent samples t-test (H). $n = 4$ organoids per condition for scRNA-seq experiments and 6–8 organoids per condition for live imaging experiments. Individual fields of view ($n = 15$ –28 per condition) were compared for statistical analysis in (K) and (L).

no effect on tumor cell viability when grown in fresh CO media (Fig. 2I). Intriguingly, GABAergic neurons account for a minor percentage of the total neurons in COs rising to approximately 15% of the total neuron population after 10 months of maturation^{25,26}. To further explore transcriptomic changes in brain cells following SCLC tumor formation in a model that includes more diverse cell types including the influence of immune cells, we analyzed a deposited scRNA-seq data set of brain stromal cells isolated from the core and edge of xenografted SCLC tumor cells in mice²⁷ (Supplementary Fig. 3A). We found evidence of chemokine expression in microglial cell clusters at the core and edge of SCLC tumors relative to sham control mice (Supplementary Fig. 3B, C). We also examined immediate early gene (IEG) expression in neurons and astrocytes at these different locations. Induction of IEG expression is a well-established proxy for neuronal activity and synaptic plasticity. Interestingly, we found a marked expression of fos, jun, and BDNF, especially in astrocyte populations at the core and edge of SCLC tumors (Supplementary Fig. 3D, E). This evidence of plasticity at the tumor-neuron interface and a GABAergic integration of SCLC cells with COs led us to examine how tumor cells and bicuculline treatment impact the spontaneous activity of COs. After a 2-week period of tumor cell growth and subsequent 72 h bicuculline treatment, we incubated COs with the calcium indicator Fluo-4 for 1 hour and conducted live imaging of spontaneous activity (Fig. 2J). The presence of H69 SCLC cells did not robustly change the frequency of spontaneous activity in COs but did result in a decrease in the amplitude of these events (Fig. 2K, L). Interestingly, bicuculline treatment resulted in a selective reduction in event frequency in COs with H69 SCLC relative to control organoids treated with bicuculline (Fig. 2K, L). Importantly, this experiment also revealed a high degree of heterogeneity in spontaneous activity within separate fields of view within individual organoids. Taken together, these findings support our electrophysiological analysis of GABAergic synapse formation on SCLC cells in hippocampal neuron preparations and suggests that this form of tumor cell integration induces a paradoxical sensitivity of the surrounding cells to the convulsant alkaloid bicuculline.

Functional changes in human neurons with SCLC

Neurological abnormalities in SCLC patients with brain metastasis include seizures^{28–30}, indicating that SCLC cells may alter the excitability of neural networks. However, the specific changes in neuron function in response to SCLC integration remain largely unexplored. Therefore, we next assessed if and how the presence of SCLC cells alters neuron function. We allowed SCLC cells to integrate with iNs for approximately 2–3 weeks before conducting experiments. We first measured the intrinsic membrane properties of iNs using a series of stepwise current injections. Here, iNs co-cultured with H69 cells revealed an increase in action potential (AP) number as a function of current step whereas H841 did not alter the intrinsic excitability of iNs (Fig. 3A, B). The resting membrane potential of iNs was not changed between these culture conditions (Fig. 3C). H69 cells also reduced the minimum current step to elicit an AP, or rheobase, of iNs and decreased iN capacitance (Fig. 3D, E). We then measured the spontaneous changes in iN membrane potential in these culture conditions. Like our current injection experiments, whole-cell current-clamp recordings of spontaneous activity revealed an increase in AP burst firing in iNs cultured with SCLC cells (Fig. 3F, G). We hypothesized that this increase in spontaneous AP generation may in part be a result of an increased rate and strength of

spontaneous synaptic vesicle fusion between neurons induced by SCLC cells, thereby increasing the amplitude of postsynaptic potentials, leading to an increased probability of AP firing. In support of this hypothesis, quantification of spontaneous excitatory postsynaptic potentials (EPSPs) revealed an increase in both EPSP frequency and amplitude in iNs co-cultured with SCLC cells (Fig. 3H–J). To directly measure if this increase in spontaneous EPSPs is indeed a result of augmented synaptic transmission between neurons, we measured miniature excitatory postsynaptic currents (mEPSCs) in the presence of tetrodotoxin to suppress AP firing. Here, we found a marked increase in the amplitude and frequency of mEPSCs between iNs co-cultured with SCLC cells (Fig. 3K, L). Acute incubation of iNs with CNQX confirmed that AMPAR activation drives spontaneous AP generation (Supplementary Fig. 4A). To test if the elevated mEPSC frequency is mediated by an increase in presynaptic release, we measured NMDAR mEPSCs in the absence of Mg²⁺ and found an elevated frequency of events whereas the amplitude of these mEPSCs remained unchanged, suggesting an elevated rate of presynaptic glutamate release between iNs with SCLC (Supplementary Fig. 4B). We then constructed rank order plots of individual AMPAR mEPSC amplitudes in these experiments to assess changes in multiplicative synaptic scaling, as this form of synaptic plasticity is distinct from Hebbian forms of plasticity^{31–34}. Rank order plots revealed a multiplicative synaptic upscaling of approximately 50% between iNs co-cultured with H841 or H69 SCLC (Fig. 3M). To address if these changes in neuron function require chronic (> 2 weeks) incubation, we measured iN function after 24 h of incubation with H69 SCLC and did not observe differences in intrinsic or spontaneous iN excitability (Supplementary Fig. 5A–F), or mEPSC frequency or amplitude (Supplementary Fig. 5G–I). These results suggest that tumor-induced remodeling of neuronal networks requires extended periods of functional integration. When we measured excitatory and inhibitory mPSCs between rat hippocampal neurons with H69 SCLC, we found an increase in the frequency of both mEPSCs and mIPSCs, whereas the amplitudes of these events were not significantly changed (Supplementary Fig. 4C, D). Taken together, these results suggest that SCLC alters neuronal excitability and strengthens iN synapse function via multiplicative scaling to increase the probability of spontaneous AP generation, thereby driving aberrant excitation throughout neural networks.

SCLC-induced synapse remodeling

Thus far, our results suggest that SCLC cells form functional synapses with neurons and drive aberrant spontaneous excitability partly by increasing the frequency and inducing multiplicative scaling of mEPSCs between neurons. We next decided to explore how SCLC cells induce multiplicative synaptic scaling between neurons. As induced neurons cultured with either H69 or H841 SCLC cells revealed similar functional phenotypes, and because H69 is an SCLC-A neuroendocrine subtype, we proceeded with uncovering SCLC-induced synaptic remodeling using H69 SCLC cells. We first asked if secreted factors from SCLC contribute to synaptic changes between neurons in the tumor microenvironment. SCLC cells are known to secrete several soluble factors that may regulate changes in neuron function including GABA, ATP, serotonin, reelin, and calcitonin gene related peptide^{6,27}. To test this hypothesis, we incubated iNs for 14 days with conditioned neurobasal media from iN-H69 co-cultures (iCM) or H69 cell monocultures (hCM) and assessed changes in synaptic transmission relative to iN-H69 co-cultures and iN monocultures without SCLC conditioned media (Fig. 4A).

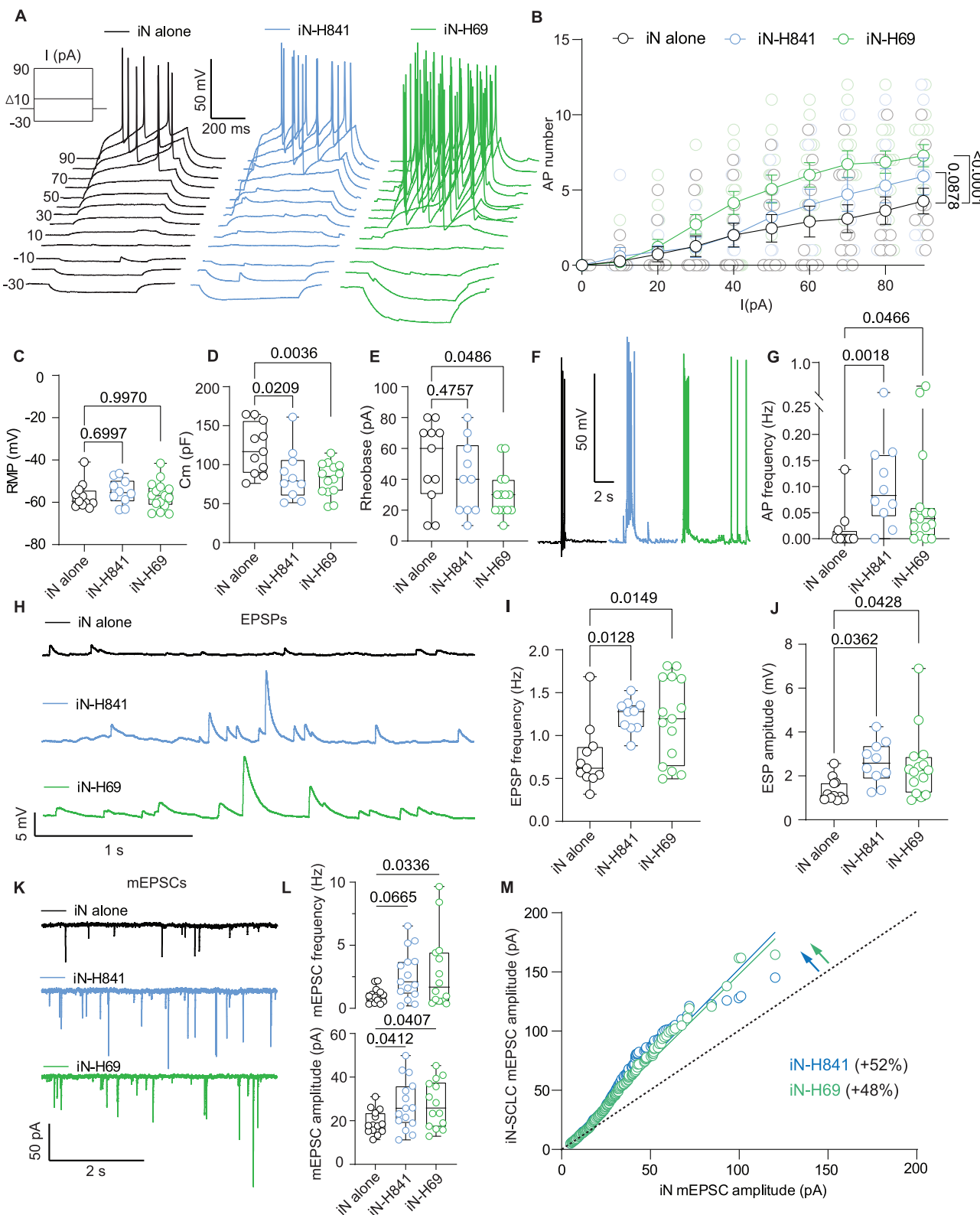


Fig. 3 | SCLC induces neuronal hyperexcitability and multiplicative synaptic scaling. **A** and **B** Representative traces of stepwise current injection and quantification of action potential number as a function of current step from -30–90 pA in iNs alone or with SCLC cells ($n = 11$ iN alone, 10 iN-H841, 14 iN-H69 cells).

C Quantification of resting membrane potential of iNs in SCLC co-culture conditions ($n = 10$ –15 cells per condition). **D** and **E** Quantification of capacitance and rheobase measurements of iNs in SCLC co-culture conditions ($n = 10$ –14 cells per condition). **F** and **G** Representative traces and quantification of spontaneous action potential firing in iNs alone relative to co-culture with SCLC cells ($n = 10$ –15 cells per

condition). **H–J** Representative traces of EPSPs between iNs and quantification of EPSP frequency and amplitude between iNs relative to iNs with SCLC ($n = 10$ –15 cells per condition). **K** and **L** Representative traces and quantification of iN mEPSC amplitude and frequency relative to iNs with SCLC cells ($n = 14$ –15 cells per condition). **M** Rank order plot of individual mEPSC amplitudes in iN-SCLC co-cultures plotted as a function of iN mEPSC amplitudes. Statistical significance was assessed by one-way ANOVA with Dunnett's multiple comparisons (**C,D,E,I,J,L**); one-way ANOVA with Dunn's multiple comparisons test (**G**); two-way ANOVA with Dunnett's multiple comparisons (**B**); simple linear regression (**M**).

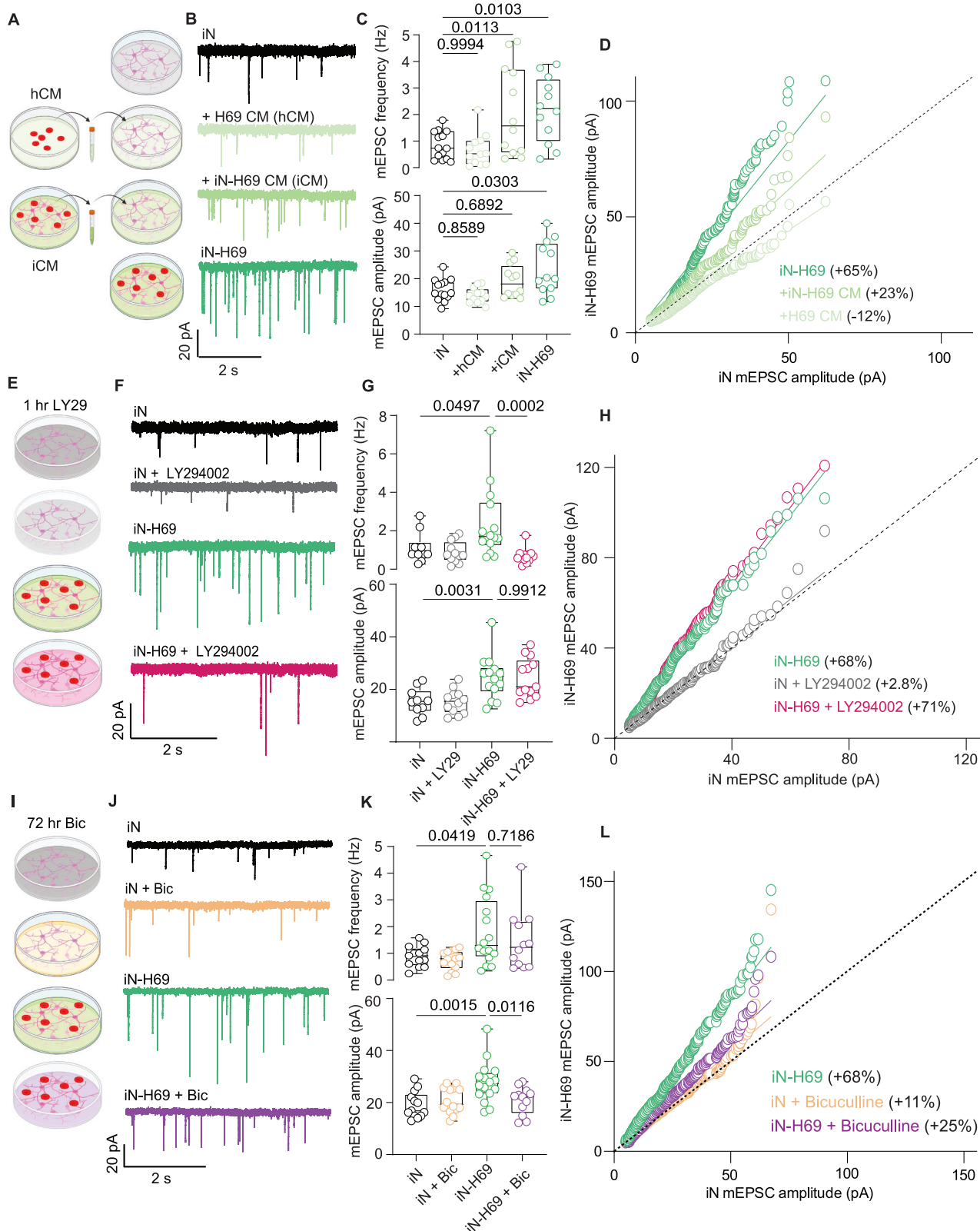


Fig. 4 | Tumor-induced multiplicative scaling is driven by physical integration of SCLC cells. A Schematic illustrating experimental strategy to test secreted factors from H69 SCLC on iN function. **B** and **C** Representative traces of iN mEPSCs from each experimental condition and quantification of mEPSC frequency and amplitude ($n = 12\text{--}14$ cells per condition). **D** Rank order plot of mEPSC amplitudes from iNs treated with conditioned media or co-cultured with H69 cells. **E** Schematic illustrating experimental strategy to test SCLC-induced PI3K signaling in iNs. **F** and **G** Representative traces and quantification of mEPSC frequency and amplitude

($n = 10\text{--}14$ cells per condition). **H** Rank order plot of mEPSC amplitudes from untreated iN-H69 co-cultures and LY294002 treated co-cultures and iN monocultures. **I** Schematic illustrating experimental strategy to test chronic bicuculline treatment on multiplicative scaling. **J** and **K** Representative traces and quantification of iN mEPSC frequency and amplitudes ($n = 12\text{--}16$ cells per condition). **L** Rank order plot of iN mEPSC amplitudes from untreated iN-H69 co-cultures and bicuculline treated co-cultures and iN monocultures. Statistical significance was assessed by two-way ANOVA with Tukey's multiple comparisons (**C,G,K**) or simple linear regression (**D,H,L**).

Here, hCM did not alter mEPSCs between iNs whereas iCM resulted in a significant increase in mEPSC frequency (Fig. 4B, C). While rank order plots revealed a modest scaling of events with iCM, the physical integration of H69 cells with iNs resulted in the most significant increase in both mEPSC amplitude and frequency (Fig. 4D). This experiment suggests that secreted factors from H69 cells in the context of neurons augment the frequency of spontaneous transmission between neurons and that the physical integration of these tumor cells is necessary to elicit multiplicative synaptic scaling. We asked if the multiplicative scaling driven by tumor cells engages a similar mechanism observed with chronic activity blockade. To test this, we incubated iN monocultures with TTX for 48 hours, a classical paradigm to induce multiplicative upscaling. In iNs however, we were surprised to find a modest but statistically significant downscaling of mEPSC amplitudes (Supplementary Fig. 6A, B). This finding suggests that tumor-induced multiplicative scaling does not involve a form of chronic activity blockade. We further explored the apparent dissociation of pathways to elicit multiplicative scaling and augmented frequency by incubated these co-cultures with the PI3 kinase inhibitor LY294002 (LY29) for 1 h (Fig. 4E, F), as a number of secreted factors in the tumor microenvironment are suggested to signal through downstream PI3K / mTOR pathways^{35–37}. Here, we found that LY29 robustly reduced the augmented mEPSC frequency between iNs with SCLC, whereas the amplitudes of these events were not reduced (Fig. 4G, H). We then asked if chronic antagonism of GABA_A receptors with bicuculline rescues this SCLC-induced aberrant upscaling between neurons. Incubation of iN-H69 co-cultures with bicuculline for 72 hours reduced H69-induced upscaling by approximately 40%, whereas incubation of iNs cultured alone with bicuculline produced a modest increase in synaptic strength of approximately 11% (Fig. 4I–L). Importantly, bicuculline treatment did not markedly reduce mEPSC frequency between neurons with H69 SCLC, unlike LY29, suggesting that synapse formation on SCLC induces multiplicative scaling between iNs while secretion of soluble factors affect mEPSC frequency. Current clamp recordings of spontaneous firing revealed that normalizing SCLC-induced synaptic scaling with bicuculline is sufficient to reduce elevated burst firing in iNs without altering the resting membrane potential (Fig. 5A–C). Bicuculline treatment also normalized intrinsic excitability phenotypes in iNs with H69 SCLC (Fig. 5D–G). Curiously, H69 SCLC also enhanced GABA_A signaling in iNs when measured following muscimol perfusion (Fig. 5H) while chronic bicuculline treatment reduced the number of Ki67 positive cells selectively in iN co-cultures (Fig. 5I). Altogether, these results suggest that SCLC cells utilize multiple strategies to alter synaptic transmission between neurons and that reducing elevated spontaneous synaptic transmission between neurons is sufficient to reduce aberrant firing patterns.

NMDA receptor activation in SCLC-remodeled circuits

A number of the currently available antiepileptic drugs used to treat seizures often augment GABAergic signaling to alleviate aberrant excitation^{38,39}. Our results currently suggest that SCLC cells can utilize GABAergic signaling mechanisms to integrate with neurons and subsequently remodel surrounding circuits to promote aberrant excitation. Therefore, we lastly explored alternative pharmacological strategies to normalize aberrant spontaneous firing between neurons that do not target GABAergic signaling. Through this lens, we hypothesized that neuronal burst firing in SCLC co-cultures is sustained by synaptic NMDA receptor activation, as these bursts consist of synchronous depolarizations that are sufficient to remove physiological concentrations of Mg²⁺ from NMDARs (Fig. 6A). Furthermore, NMDAR activation has been previously shown to regulate synchronous bursting in cortical neurons and emerges at later developmental stages in these Ngn2 derived preparations^{14,15}. To test this hypothesis, we perfused the competitive NMDAR antagonist AP5 while continuously recording spontaneous firing activity in human neurons with or without H69 SCLC (Fig. 6B). Application of AP5 markedly decreased the augmented spontaneous AP frequency in SCLC co-cultures (Fig. 6C, D). This decrease in firing was not a result of a decrease in the number of burst initiations (Fig. 6E). Instead, the decrease in AP frequency following AP5

application was a result of a reduction in the number of APs per burst (Fig. 6F), consistent with NMDA receptor activation requiring sufficient depolarization of the postsynaptic membrane. This result suggests that AMPAR-mediated synaptic NMDAR activation sustains SCLC-induced aberrant burst firing in iNs. Incubating iN-H69 co-cultures with AP5 for one week also resulted in a reduction in tumor cell density (Supplementary Fig. 7A) while chronic AP5 did not alter spontaneous firing dynamics in iN-H69 co-cultures (Supplementary Fig. 7B), consistent with the requirement of PV neurons in regulating neuronal network firing setpoints⁴⁰. We then tested whether memantine, an FDA-approved uncompetitive NMDAR open channel blocker, could also reduce aberrant burst firing in this SCLC-iN system. We followed the same experimental protocol as described with AP5 and found that memantine perfusion also reduced the spontaneous AP frequency in human neurons with H69 SCLC (Fig. 6G, H). Interestingly, memantine modestly but consistently reduced both the spike number per burst as well as the number of burst initiations (Fig. 6I, J). Taken together, these results suggest that NMDA receptor activation sustains aberrant spontaneous activity between human neurons within the SCLC micro-environment and therapeutics that do not target GABAergic signaling, such as memantine may be effective in ameliorating this aberrant excitation.

Discussion

SCLC largely originates from pulmonary neuroendocrine epithelial cells, which can normally form synaptic contacts with neurons⁶. In their neoplastic counterpart, this capacity for synapse formation appears to be maintained, as we show here, and may play a role in the propensity of SCLC to metastasize to the brain, raising intriguing questions on the types of interactions SCLC cells may establish with the brain neural micro-environment following metastasis^{41–43}. Glioma cells can also form functional synapses with neurons and electrically integrate into surrounding neural networks^{10,11}. These neuron to glioma synapses are suggested to be largely mediated by postsynaptic expression of α -amino-3-hydroxy-5-methyl-4-isoxazolepropionic acid (AMPA) receptors that depolarize glioma cells and ultimately promote tumor growth in the brain^{10,11} although recent work has also documented evidence for GABAergic synapse formation on diffuse midline glioma cells⁴⁴. Our results suggest that SCLC cells can express multiple postsynaptic receptor subunits and preferentially select for components of GABAergic transmission with central neurons. Transcriptomic profiles of H69 in COs and electrophysiological analysis of H69 SCLC grown in mixed and largely homogeneous neuron model systems support this conclusion. While we note this predilection of H69 SCLC, which maintains a neuroendocrine SCLC subtype, and H841, a non-neuroendocrine subtype, it remains to be seen whether synaptic integration is a limited or general property amongst the currently recognized 5 SCLC subtypes (neuroendocrine A, A2, and N; and non-neuroendocrine P and Y). Additionally, transcriptomic changes in tumor cells invading nervous tissue, not directly related to synapse formation, also contribute to the proliferation of cancer cells in the brain. We reveal evidence for AP-like waveforms in neuroendocrine H69 SCLC, consistent with recent literature exploring the intrinsic excitability of SCLC subtypes⁴⁵. Furthermore, these tumoral synapses were not detected on a majority of SCLC cells and often did not exceed 40 pA of current. Future studies exploring the underlying mechanisms between variability in synapse type and strength between different metastatic tumors will provide further evidence regarding how the intrinsic transcriptional profiles of tumor cells relate to the propensity for a cancer cell to metastasize to the brain and form functional synapses with neurons.

Consistent with previous work on neuron-to-glioma synapses, the neuron-to-SCLC synapses described here facilitate in response to repetitive stimulation¹¹, indicating a relatively low presynaptic release probability (P_r)⁴⁶. This low P_r between neuron-to-SCLC synapses is likely due to a small presynaptic RRP size, indicating immature synapse formation on SCLC, as these low P_r neuron-to-SCLC synapses are in robust contrast to the high release probability of evoked GABAergic synaptic currents and glutamatergic synapses formed between neurons^{47,48}. However, additional

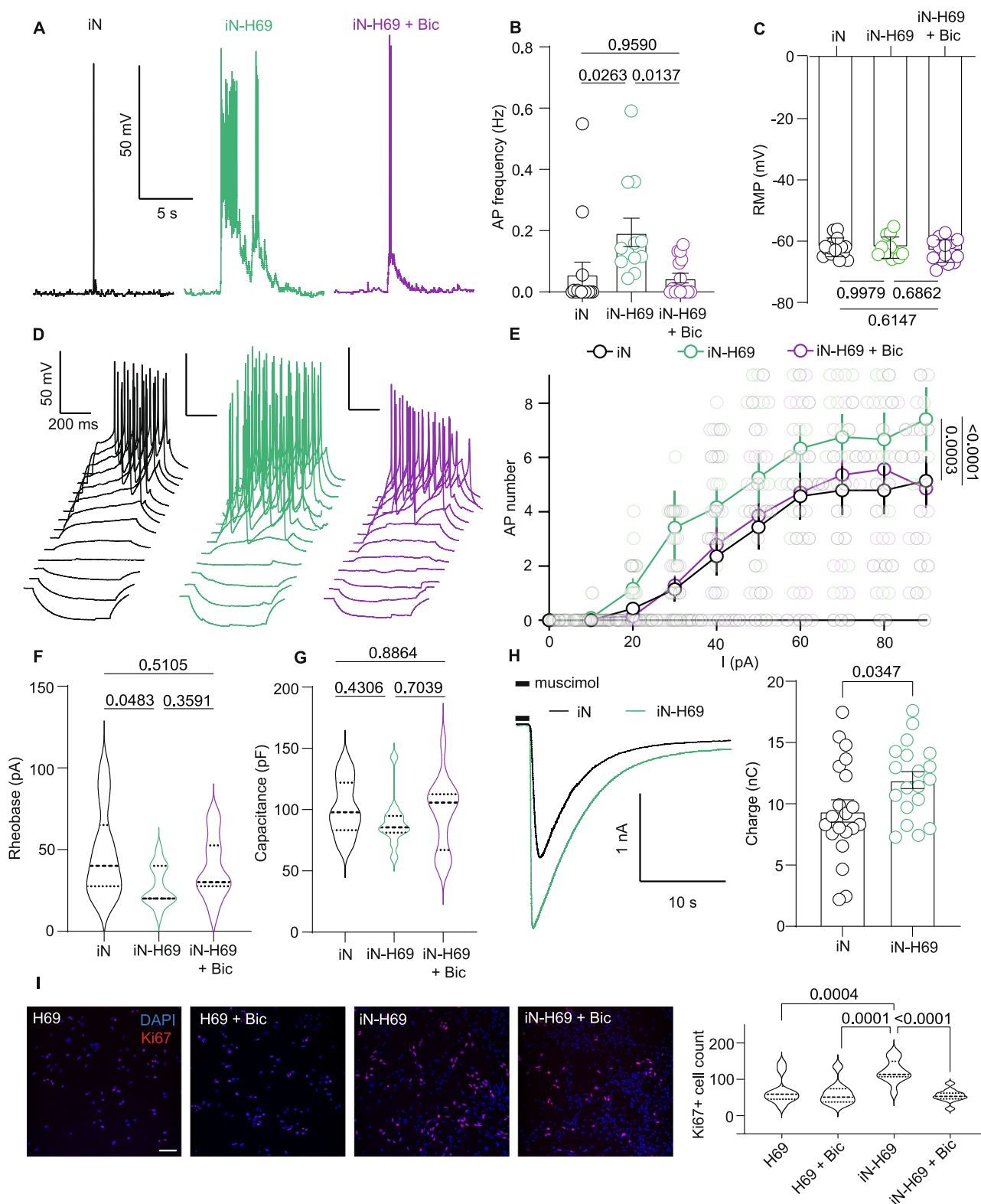


Fig. 5 | Bicuculline treatment normalizes iN-H69 excitability phenotypes and reduces H69 proliferation in the context of neurons. **A** and **B** Representative traces and quantification of spontaneous firing activity in iN monocultures, iN-H69 co-cultures and iN-H69 treated with bicuculline ($n = 12$ –15 cells per condition). **C** Quantification of resting membrane potential in iN monocultures, iN-H69 and iN-H69 treated with bicuculline ($n = 12$ –15 cells per condition). **D** Representative traces of stepwise depolarization of iN monocultures, iN-H69 co-cultures and co-cultures treated with bicuculline. **E** Quantification of action potential number as a function of current step ($n = 12$ –14 cells per condition). **F** and **G** Quantification of rheobase and capacitance measurements from iN monocultures, iN-H69 co-

cultures and bicuculline-treated iN-H69 co-cultures ($n = 12$ –14 cells per condition). **H** Example trace of muscimol perfusion in iN monocultures and iN-H69 co-cultures and quantification of total charge following muscimol ($n = 19$ –20 cells per condition). **I** Example images of Ki67 and DAPI staining in H69 monocultures and iN-H69 co-cultures treated with bicuculline and quantification of Ki67+ cells per field of view ($n = 10$ –12 FOV per condition). Scale bar = 100 μ m. Statistical significance was assessed by one-way ANOVA with Tukey's multiple comparisons (**B,C,F,G**); two-way ANOVA with Tukey's multiple comparisons (**I**); two-way ANOVA with Dunnett's multiple comparisons (**E**); independent samples t-test (**H**).

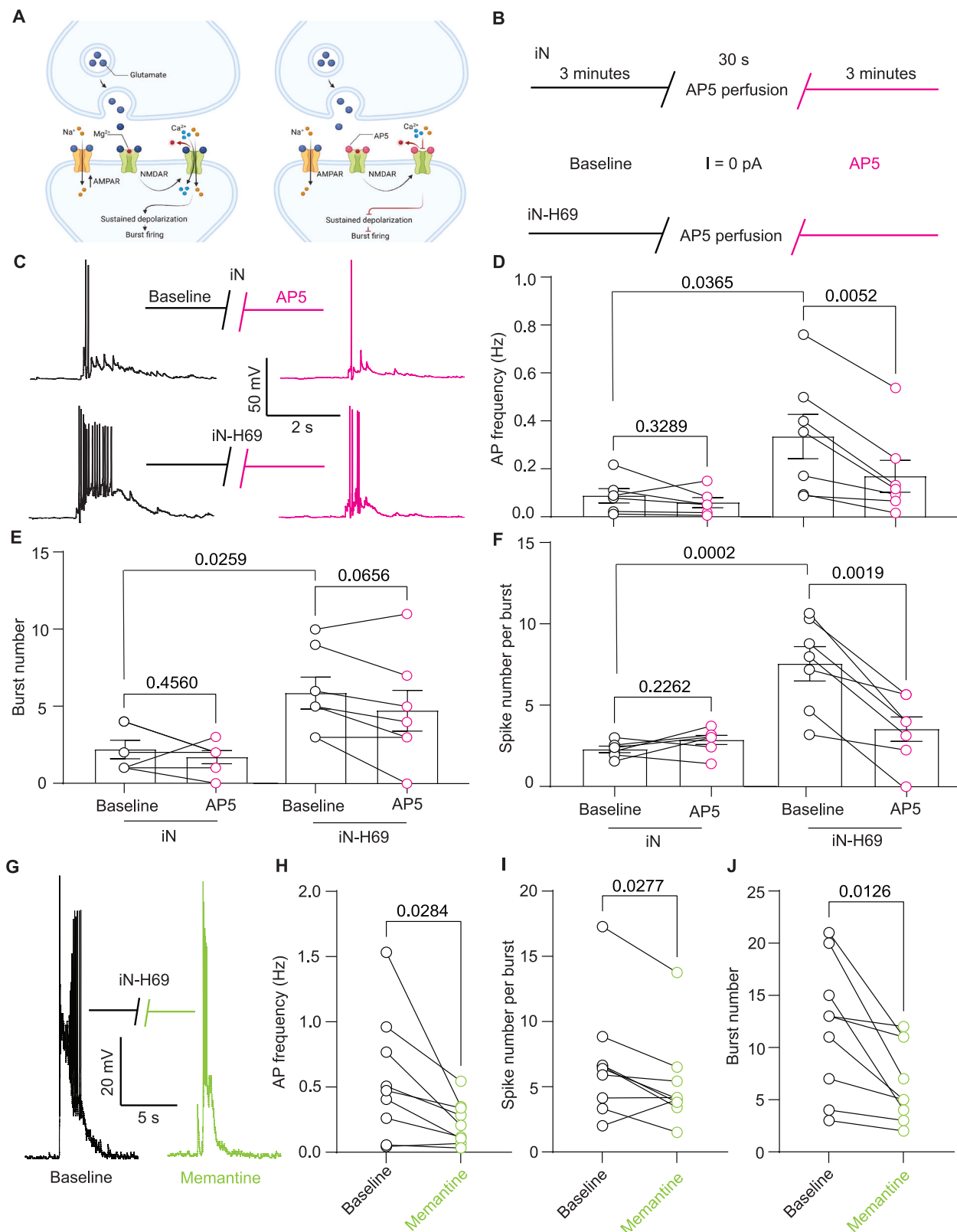


Fig. 6 | NMDAR activation sustains aberrant burst firing in human neurons with SCLC. A Schematic illustrating the proposed role of NMDA receptor activation in sustaining elevated spontaneous firing in neurons with SCLC. B and C Pharmacological strategy to test NMDAR activation in neuronal burst firing and example traces of spontaneous bursts before and after AP5 perfusion in iN monocultures (top traces) and iN-H69 co-cultures (bottom traces). D–F Quantification of AP frequency, burst number, and spike number per burst in iN monocultures or iN-SCLC co-cultures before and after AP5 perfusion ($n = 6$ –7 cells per condition).

G Representative trace of burst firing in iN-H69 co-culture before and after memantine perfusion. H–J Quantification of AP frequency, spike number per burst, and burst number in iN-H69 co-cultures before and after memantine perfusion ($n = 9$ cells). All summary graphs show mean \pm SEM. Statistical significance was assessed by paired samples t-test for before-after AP5 comparisons (D,E,F,H,I,J); two-way ANOVA with Tukey's multiple comparisons between iN and iN-H69 conditions (D,E,F).

possibilities regulating this functional distinction, such as altered pre-synaptic calcium buffering relative to neuronal synapses should be considered⁴⁹. This functional distinction may represent a vulnerability of SCLC progression in the brain. Future work exploring how synapses on SCLC can be selectively targeted in the brain will provide valuable insight into this potential therapeutic avenue. Recent research explored this avenue using modified rabies virus to selectively induce apoptosis in tumor cell-connected neurons and revealed a reduction in glioma cell number⁵⁰. Tumor cells in the neuronal microenvironment can utilize numerous mechanisms to both integrate into neural networks and subsequently alter neuron function. Due to the intrinsic plasticity of SCLC cells, it is possible that the brain microenvironment promotes cell-state transitions to synapse-forming cell types, since such phenotypic changes have been observed in SCLC tumors undergoing treatment⁵¹. In addition to direct synapse formation on tumor cells, secreted factors from SCLC and other cancer types in the brain may play a central role in dysregulating neuron function. Synaptogenic factors such as thrombospondin-1 have been shown to be upregulated in the tumor microenvironment⁹. The secreted glycoprotein reelin has also been recently suggested to promote SCLC metastasis, further highlighting the complex signaling induced by secreted factors from tumor cells²⁷. Our data highlight downstream PI3K signaling in neurons as a potential pathway activated by candidate secreted factors from SCLC cells, suggesting a potential target to alleviate aberrant synaptic plasticity in the tumor microenvironment.

Additional work has explored the reciprocal effects of primary brain tumors on neuron function and uncovered neuron activity-dependent mechanisms that drive glioma proliferation in brain largely through increased neural excitability, paracrine signaling, and dysregulated synaptic communication between neurons^{52–57}. These findings complement clinical reports of seizures in patients with glioma and suggest that seizures in patients with cancers in the brain may be a result of aberrant electrochemical communication between neurons and tumor cells^{9,28,30,38}. Our analysis of neuron function in the presence of SCLC revealed that SCLC cells alter the excitability, spontaneous firing properties, and synaptic function of iN cells. While the increase in spontaneous neurotransmission in the presence of SCLC is similar to neuronal phenotypes elicited by glioma, our analysis indicates that the alterations in excitatory synapse function induced by SCLC is global in nature. In contrast to Hebbian forms of plasticity, this homeostatic-like scaling indicates that SCLC cells strengthen all neuronal synapses in a multiplicative manner as opposed to a subset of relatively stronger or weaker synapses^{31,32}. Whether other cancers, such as glioma, induce homeostatic or Hebbian forms of synaptic plasticity to alter neural excitability will be crucial to understand the underlying mechanisms that drive aberrant neuronal plasticity. Normally, the induction of synaptic upscaling triggers compensatory mechanisms in firing activity to maintain an intrinsic neuronal setpoint. In contrast, the SCLC-induced synaptic scaling shown here corresponds to an increase in neuron firing, indicative of a homeostatic network collapse⁵⁸. This failure to maintain neuronal homeostasis has also been documented in models of early stage Alzheimer's disease^{58,59}, and suggests that failure to induce compensatory mechanisms drives aberrant neuronal activity induced by SCLC.

In addition to homeostatic plasticity, we show that aberrant neuronal excitation in the SCLC microenvironment can be rapidly normalized by the NMDAR antagonists AP5 or memantine. Reducing SCLC-induced multiplicative scaling between neurons using chronic bicuculline was also an effective approach to normalize aberrant firing and suggests that treating subthreshold synaptic phenotypes induced by tumor cells may be an effective strategy in treating neurological symptoms of brain metastasis. Metabotropic GABA signaling through GABA_A receptor in the tumor microenvironment was also shown to promote tumor growth, highlighting the diversity of neurotransmitter signaling in tumor pathobiology⁶⁰. While alternative antiepileptic drugs that augment GABAergic signaling may also be effective in normalizing neurological phenotypes in patients with SCLC brain metastasis, our data indicate that SCLC cells utilize GABAergic synapse formation to integrate with neurons. Interestingly, previous work

has demonstrated that GABAergic agonists propofol and muscimol can increase tumor growth whereas GABA_AR antagonists bicuculline and flumazenil can suppress pancreatic and metastatic neuroendocrine tumors, respectively^{61–63}. Recent work has shown functional GABAergic synapse formation on diffuse midline gliomas and growth-promoting effects of the benzodiazepine lorazepam⁴⁴. Importantly, the effectiveness of these treatments is dependent on tumor cell identity and the context of the surrounding microenvironment. Nonetheless, future studies examining how GABAergic agonists impact tumor growth in the brain and alternative therapeutic strategies to normalize aberrant excitation may prove beneficial in treating patients with SCLC brain metastasis.

While this study demonstrates synapse formation on small cell lung cancer in vitro, future studies exploring the synaptic integration of SCLC in mouse models of spontaneous brain metastasis will provide further insight into the pathophysiology of tumor cell integration in vivo. Additionally, while we characterized the functional integration of two human SCLC cell lines, future work exploring additional SCLC cell types will shed light on the generalizability of our findings to the diverse molecular profiles of SCLC tumors. While we show evidence for tumor cell-induced synaptic remodeling between human neurons that is sustained by NMDA receptor activation, future trials exploring the therapeutic efficacy of the in vitro pharmacology described here will also be needed to validate the clinical application of these results.

Methods

Cell culture

H1 human ES cells (WiCell, WA01) were maintained in mTeSR (STEMCELL #100–0276) and passaged using ReLeSR (STEMCELL #100–0483) in Matrigel (Corning #354234) coated 6-well plates. H69 SCLC cells (NCI-H69, human lung carcinoma) were maintained in RPMI media (ThermoFisher #11875093) with 5% FBS and 1% Penicillin-Streptomycin (Gibco #15140122). H841 SCLC (NCI-H841, human lung carcinoma) was maintained in DMEM/F12 (ThermoFisher #11320033) with 5% FBS and 1% P/S and passaged using Trypsin-EDTA (Gibco #25200114). Mouse glial cells were isolated from P1-P2 CD1 mouse pup forebrains and dissociated using Papain digestion and maintained in DMEM high glucose (Gibco #10569044) with 5% FBS and 1% P/S. Mouse glial cells were passaged 1–2 times using Trypsin before seeding on Poly-D-Lysine (ThermoFisher #A3890401) coated glass coverslips for iN co-culture. All cells were incubated at 37 °C with 5% CO₂ and passaged at 80% confluence.

Virus generation

Lentiviral vectors were generated using HEK-293T cells (ATCC) as previously described⁶⁴. Briefly, HEK cells were passaged the day before transfection in antibiotic-free DMEM media to reach 70–80% confluence at the time of transfection. HEK cells were then transfected with lentiviral packaging plasmids pRSV-Rev, pMDLg/pRRE, pCMV-VSV-G and transgene expression constructs using Fugene6 transfection reagent (Promega #E2691) and diluted in Opti-MEM (ThermoFisher #31985062). HEK cells were incubated with transfection complexes for 24 hours, and then the media was changed to collection media and harvested after 36–48 hours. Lentiviral supernatants were centrifuged at 2000 rpm for 15 min to remove cellular debris. Supernatants were then aliquoted and stored at -80 °C.

Generation of induced human neuron (iN) cells

iN cells were generated as previously described^{14–16,64}. Briefly, on day 0, H1 ES cells (WA01) were dissociated using Accutase (Gibco #A1110501) and replated as a single cell suspension in mTeSR in the presence of 10 μM Rho-associated protein kinase inhibitor (ROCKi) (STEMCELL #72304), Ngn2 and rtTA lentivirus, and 8 μg/mL polybrene (Sigma #TR-1003) to increase transduction efficiency. After 24 hours, the media was changed to induction media using DMEM/F12 containing 1X N2 and non-essential amino acids (ThermoFisher #11140076), 1% P/S, 2% B27 supplement (Gibco #17504-010), insulin (Sigma #11070-73-8), 2 μg/uL doxycycline (Sigma #D9891), Recombinant human/murine/rat BDNF (PeproTech #45002), Recombinant

human NT-3 (Peprotech #45003), and mouse Laminin (Invitrogen #23017015) (all 1 µg/mL). On day 2, the induction media were changed to selection media made using the same reagents as induction media with the addition of 1 µg/mL puromycin (Sigma #P8833). On day 4, developing iNs were gently dissociated using Accutase (Gibco #A1110501) and re-plated on glass coverslips with pre-plated mouse glial cells and maintained in neurobasal plus media (Gibco #A3582901) containing 1X GlutaMAX supplement (Gibco #35050061), B27 supplement, 5% FBS, and 1% P/S with BDNF, NT-3, mLaminin, and doxycycline. Approximately 70,000 iN cells were re-plated into one well of a 24-well plate. Following re-plating, half of the neurobasal media was changed every 3 days. Supplements BDNF, NT-3, Laminin, and doxycycline were maintained in neurobasal media until day 15. After day 15, half of the neurobasal media was changed every 5 days without the addition of neurotrophic supplements and doxycycline.

Generation of cerebral organoids (COs)

COs were generated as previously described^{22,65}. Briefly, H1 hESCs were grown until colonies reached 80% confluence. Cells were then plated in low-attachment 96-well plates (9000 cells per 150 mL of STEMdiff Neural Induction Medium (STEMCELL #05835). Embryoid bodies were fed every other day for 6–7 days; medium contained 50 mM ROCKi for the first 4 days. To initiate neural rosette formation, embryoid bodies were transferred to Matrigel-coated (Corning #354277) 6-well plates where they received daily medium changes (STEMdiff Neural Induction) for 6–7 days. Neural rosette clusters were transferred to droplets of Matrigel (Corning #356234) by pipetting into cold Matrigel on a sheet of Parafilm. Droplets were solidified at 37 °C and were subsequently grown without agitation for 4 days in differentiation medium type I²². Following this stationary growth phase, the tissue droplets were transferred to an orbital shaker containing differentiation medium type II²².

SCLC-CO co-culture and imaging

COs (4–6 weeks old) were co-cultured together with mKate2-labeled H69 SCLC cells in one well of a 24-well plate at a concentration of 100,000 H69 cells per organoid. For the first 24 hours, co-cultured samples were maintained in RPMI media with 5% FBS and 1% P/S at 37 °C without agitation. Following this initial 24 hours, organoids were gently washed in PBS and transferred to a single well of a 6-well plate containing 3 mL of organoid differentiation medium type II (17) and placed on an orbital shaker for an additional 24 hours. For live fluorescent imaging, COs were imaged for tumor burden prior to fluo-04 incubation. COs were incubated in 10 µM fluo-04 for one hour at 37 °C. Organoids were then rinsed in 1 mL of PBS and then placed in modified Tyrode's during live imaging. Approximately 3–4 fields of view were captured for each organoid depending on CO size. Individual fields of view were selected at random within individual organoids.

Single-cell RNA-sequencing and analysis

After 48 h of incubation, two-dimensional cultures and tumor-bearing organoids were dissociated into single-cell suspensions with collagenase type II. Cells were filtered through a 40 µm strainer and resuspended in ice-cold PBS/2%BSA. Cell viability was checked at every step of the process by Trypan Blue Exclusion. Samples were processed through the particle-templated instant partition sequencing (PIP-seq) platform using Fluent BioSciences' PIPseq™ T2 3' Single Cell Capture and Lysis Kit v2.0⁶⁶.

Cells used for single-cell RNA seq were prepared according to the PIPseq single-cell capture and lysis user guide. A cell suspension was prepared in the cell suspension buffer provided from the PIPseq™ T2 3' single cell capture and Lysis Kit v2.0. Cells were added to Pre-templated Instant Partitions (PIPs) and vortexed. Stable emulsions containing captured mRNA were subsequently washed, and cDNA synthesis was conducted according to the manufacturer's instructions. cDNA products were submitted to the Vanderbilt University VANTAGE core where whole genome sequencing (WGS) library generation was performed. cDNA libraries were sequenced on an Illumina NovaSeq 6000 instrument at a read depth of 100 million.

For gene preprocessing and filtering, all genes expressed in less than three cells were removed. Cells expressing fewer than 200 genes or having more than 20% mitochondrial gene expression were also removed. To determine the extent of cell cycle regulation in gene expression space, we used a list of cell cycle markers from Tirosh et al. 2015 loaded with Seurat. The genes in this list were associated with either G1, G2M, or S phase using the *CellCycleScoring* to assign a score. For the remaining preprocessing analysis for both 2D H69 and CO H69 samples Seurat was used: total counts were normalized by cell, then data were log transformed. Highly variable genes were determined with Seurat *selection.method* = "vst", and *nfeatures* = 3000. A PCA, and UMAP clustering were then calculated using *FindNeighbors* and *FindClusters* with *resolution* = 0.5. Tumor cell cluster within the CO H69 sample was selected for further analysis to compare to the 2D H69 sample.

Downstream analysis for both sample comparisons was done by converting Seurat objects for both samples into AnnData objects (using *srt_to_aadata*) to use in Scanpy. Ranking for highly differential genes in each cluster was performed using Scanpy's *sc.tl.rank_genes_groups* using the *wilcoxon* method from Soneson & Robinson⁶⁷. *Wilcoxon* test returns p values for all differential gene expression comparison between both samples. Visualization for violin plots for both 2D H69 and CO H69 samples were created using Scanpy's *rank_genes_groups_violin* and visualized using GraphPad Prism with selected proliferative markers Ki67 and PCNA, synaptic cell adhesion markers, GABAergic synapse related genes and glutamatergic synapse related genes. For data and code availability, any additional information required to reanalyze the data reported in this paper is available from the lead contact upon request.

Primary rat hippocampal neuron culture

Primary rat hippocampal neurons were isolated from P0-P1 Sprague-Dawley rat pups of either sex. After hippocampal dissection in cold Hanks balanced salt solution (Sigma #H2387-10X1L) with 20% FBS, the tissue was enzymatically digested with trypsin in the presence of 0.5 mg/ml DNase (Sigma #D5025-375KU) for 10 min at 37 °C. Hippocampi were then mechanically dissociated and plated on Matrigel coated glass coverslips in MEM (Gibco #51-200-038) containing 10% FBS, 0.2 g/L NaHCO₃, 0.1 g/L Transferrin (Sigma #616420-100MG), 2 mM L-glutamine, 20 mg/L insulin, and 5 g/L D-glucose. The following day, the media was changed to MEM containing 5% FBS, 5 mM L-glutamine, 10 mL/0.5 L B27 supplement and 4 µM cytosine arabinoside (Sigma #C1768). On day 4, half of the media was changed to reduce the final cytosine arabinoside to 2 µM. Hippocampal cultures were incubated at 37 °C and 5% CO₂. All experiments using animals performed in this study were approved by the Institutional Animal Care and Use Committee at Vanderbilt University. We have complied with all relevant ethical regulations for animal use. Animal health was regularly monitored by animal facility veterinary staff at Vanderbilt University.

SCLC co-culture

SCLC cells were dissociated using trypsin and resuspended in neuronal media and counted using an automated cell counter with Trypan blue correction. Approximately 25,000 SCLC cells were added to each well of a 24-well plate containing rat or human neuron cultures. SCLC cells were added to rat hippocampal neurons at day 6 and experiments were performed 10 to 15 days later. SCLC cells were seeded when iN cells were 20–25 days old and incubated for 15–20 days before experiments were conducted.

Cell viability and cytotoxicity assay

H69 cells were seeded in 96-well plates (5000 cells per well) either alone, as tumor organoids (TO; 20 µL Matrigel), or within COs (in 20 µL Matrigel). Upon seeding, cells were treated with DMSO or bicuculline (BIC; 20 µM) for 6 days; on Day 3, exhausted medium was replaced with fresh medium containing DMSO or BIC. On Day 6, medium was removed and each well received 90 µL RPMI (with 10% FBS and 1% P/S) plus 10 µL alamarBlue Reagent (Thermo Scientific). Following a 3 hour incubation, relative

fluorescence units (RFU) were measured on an Agilent BioTek Synergy H1 multi-mode microplate reader using an excitation wavelength of 560 nm and an emission wavelength of 590 nm.

Conditioned media

H69 cells were cultured alone in T75 flasks or with induced neurons in neurobasal plus media. Neurobasal plus media was harvested every 48 hours from H69-iN co-cultures or H69 monocultures. The conditioned media was briefly centrifuged for 5 min at 300xg to remove cell debris and added to monocultures of induced neurons. Adjacent wells of SCLC-iN co-cultures and iN monocultures from the same preparation were used as positive and negative controls, respectively. Induced neurons were incubated for 14 days in replenished conditioned media prior to electrophysiology experiments.

Electrophysiology

Whole cell voltage clamp recordings were conducted using 4-6 MΩ borosilicate glass patch pipettes filled with internal solution containing (in mM): 115 Cs-MeSO₃, 20 tetraethylammonium-Cl, 10 HEPES, 10 CsCl, 10 QX-314, 5 NaCl, 4 Mg-ATP, 0.6 EGTA, 0.3 Na₃GTP. The pH was adjusted to 7.3 using CsOH with an osmolarity of 290-300 mOsm. QX-314 was included in voltage-clamp pipette solution to block AP generation in patched cells. Whole cell current-clamp recordings were conducted using the internal solution (in mM): 110 K-Gluconate, 20 KCl, 10 NaCl, 10 HEPES, 4 Mg-ATP, 0.3 Na₃GTP, 0.6 EGTA. The pH was adjusted to 7.3 using KOH and osmolarity was in the range of 285-290 mOsm. A modified Tyrode's solution was used as the external solution containing (in mM) 150 NaCl, 10 D-Glucose, 10 HEPES, 4 KCl, 2 CaCl, 1.25 MgCl at pH 7.4 and 310 mOsm. Memantine (Tocris #0773), AP-V (Sigma #A8054) or CNQX (Sigma #C239) were added to the modified Tyrode's in current clamp configurations for acute perfusion experiments. Evoked recordings were conducted using a bipolar electrode immersed in the external solution and delivered 35 mA pulses from a stimulus isolator. Evoked recordings were conducted at 1X gain, while mPSC recordings were conducted at 10X gain. Quantization of amplitudes resulted in some identical amplitude measurements despite originating from separate traces. All cells were held at -70mV for voltage-clamp recordings. To isolate eEPSCs, 50 μM bicuculline (Sigma #14340) and 20 μM AP-V were added to the external bath solution. To isolate eIPSCs, 20 μM AP-V and 10 μM CNQX were added to the external bath solution. Isolated mEPSC were recorded in 1 μM TTX (Tocris #1078), 50 μM bicuculline and 20 μM AP-V. RRP events were evoked using 500 mM sucrose in modified Tyrode's solution containing 2 mM CaCl and 1.25 mM MgCl in whole-cell voltage-clamp configuration. Evoked voltage-clamp and current-clamp recordings were analyzed using Clampfit 10.2. mEPSCs were analyzed using mini analysis (Synaptosoft).

Immunocytochemistry

Coverslips were fixed in PBS containing 4% PFA and 4% sucrose for 20 min at room temperature. Following 3 washes in PBS, coverslips were then incubated in a permeabilization solution containing 0.2% Triton-X in PBS for 30 min at room temperature. Coverslips were then washed in PBS and incubated in a blocking solution containing 1% bovine serum albumin and 2% normal goat serum for 1 h at room temperature. Coverslips were then incubated in primary antibodies diluted in the blocking solution in a humidified chamber overnight at 4 °C: Anti-vGAT 1:500 (Synaptic Systems #131-008) and Anti-Gephyrin 1:200 (Synaptic Systems #147-021). Coverslips were then washed in PBS and incubated in species appropriate Alexa fluor secondary antibodies for 2 h at room temperature. Coverslips were then washed and mounted on glass microscope slides in Aqua-Poly/Mount (Fisher #NC9439247) and imaged using a Zeiss LSM 710 with a 63X oil immersion objective.

Live fluorescence imaging

H69 SCLC cells were transduced as 2D monocultures with lentiviral vectors containing iGluSnFR. Transduced H69 cells were then dissociated after

24 hours using Trypsin, added to rat hippocampal cultures on DIV 6 and imaged on DIV 18. Live imaging experiments were conducted in unmodified Tyrode's buffer containing 2 mM CaCl and 1.25 mM MgCl. Fluorescence was recorded using a Nikon Eclipse TE2000-U inverted microscope equipped with a 60x Plan Fluor objective, a Lambda-DG4 illumination system with FITC excitation and emission filters, and an Andor iXon + back-illuminated EMCCD camera. Images were acquired at 50 Hz to resolve fast spiking glutamatergic peaks. Evoked responses were elicited using a bipolar electrode immersed in the external solution and delivered 35 mA pulses from a stimulus isolator. Imaging synapse formation in iN-SCLC co-cultures was conducted using a Nikon A1-R Eclipse Ti confocal microscope in resonant scanning with a 60x Plan Apochromat Lambda objective.

Statistics and reproducibility

All statistical analyzes were conducted using GraphPad Prism 9.1. No power analyzes were conducted to determine sample sizes in these experiments as the effect sizes were unknown. Sample sizes for electrophysiology experiments were based on previous studies in molecular neuroscience and performed in at least two independent neuron cultures. For comparison of two groups in a before-after experimental paradigm, paired-samples *t*-test were used. For comparison of two independent groups, independent samples *t*-test was used. If both groups were not normally distributed, or *N* was too small for normality calculations, non-parametric tests were used for statistical comparisons. Comparisons of gene expression in scRNA-seq. graphs were made using Wilcoxon-signed rank test. Comparison of more than two conditions was determined using One-way ANOVA while two-way ANOVA was used to compare more than two groups with two independent variables with post-hoc correction. All summary graphs display mean ± SEM unless otherwise stated.

Reporting summary

Further information on research design is available in the Nature Portfolio Reporting Summary linked to this article.

Data availability

All relevant raw data associated with the manuscript are located in the Supplementary data 1 file. RNA sequencing data are available under the accession ID: GSE305403.

Received: 9 July 2025; Accepted: 6 October 2025;

Published online: 13 November 2025

References

1. Bao, S. et al. Stem cell-like glioma cells promote tumor angiogenesis through vascular endothelial growth factor. *Cancer Res.* **66**, 7843–7848 (2006).
2. Goustin, A. S., Leof, E. B., Shipley, G. D. & Moses, H. L. Growth factors and cancer. *Cancer Res.* **46**, 1015–1029 (1986).
3. Kaal, E. C. A., Niël, C. G. J. H. & Vecht, C. J. Therapeutic management of brain metastasis. *Lancet Neurol.* **4**, 289–298 (2005).
4. Riihimäki, M. et al. Metastatic sites and survival in lung cancer. *Lung Cancer* **86**, 78–84 (2014).
5. Nakazawa, K. et al. Specific organ metastases and survival in small cell lung cancer. *Oncol. Lett.* **4**, 617–620 (2012).
6. Noguchi, M., Furukawa, K. T. & Morimoto, M. Pulmonary neuroendocrine cells: physiology, tissue homeostasis and disease. *Dis. Model. Mech.* **13**, 46920 (2020).
7. Murray, N. & Turrisi, A. T. 3rd. A review of first-line treatment for small-cell lung cancer. *J. Thorac. Oncol. Publ. Int. Assoc. Study Lung Cancer* **1**, 270–278 (2006).
8. Huang-Hobbs, E. et al. Remote neuronal activity drives glioma progression through SEMA4F. *Nature* **619**, 844–850 (2023).
9. Krishna, S. et al. Glioblastoma remodelling of human neural circuits decreases survival. *Nature* **617**, 599–607 (2023).

10. Venkataramani, V. et al. Glutamatergic synaptic input to glioma cells drives brain tumour progression. *Nature* **573**, 532–538 (2019).
11. Venkatesh, H. S. et al. Electrical and synaptic integration of glioma into neural circuits. *Nature* **573**, 539–545 (2019).
12. Savchuk, S. et al. Neuronal activity-dependent mechanisms of small cell lung cancer pathogenesis. *Nature* (2025) <https://doi.org/10.1038/s41586-025-09492-z>.
13. Sakthivelu, V. et al. Functional synapses between neurons and small cell lung cancer. *Nature* (2025) <https://doi.org/10.1038/s41586-025-09434-9>.
14. Zhang, Y. et al. Rapid single-step induction of functional neurons from human pluripotent stem cells. *Neuron* **78**, 785–798 (2013).
15. Uzay, B. et al. Neurotransmitter release progressively desynchronizes in induced human neurons during synapse maturation and aging. *Cell Rep.* **42**, 112042 (2023).
16. Houcek, A. et al. CRISPR-Cas9 editing of synaptic genes in human embryonic stem cells for functional analysis in induced human neurons. *STAR Protoc.* **5**, 103089 (2024).
17. Menuz, K., Stroud, R. M., Nicoll, R. A. & Hays, F. A. TARP auxiliary subunits switch AMPA receptor antagonists into partial agonists. *Science* **318**, 815–817 (2007).
18. Cokić, B. & Stein, V. Stargazin modulates AMPA receptor antagonism. *Neuropharmacology* **54**, 1062–1070 (2008).
19. Stevens, C. F. & Tsujimoto, T. Estimates for the pool size of releasable quanta at a single central synapse and for the time required to refill the pool. *Proc. Natl. Acad. Sci. USA* **92**, 846–849 (1995).
20. Rosenmund, C. & Stevens, C. F. Definition of the readily releasable pool of vesicles at hippocampal synapses. *Neuron* **16**, 1197–1207 (1996).
21. Burlingham, S. R. et al. Induction of synapse formation by de novo neurotransmitter synthesis. *Nat. Commun.* **13**, 3060 (2022).
22. Linkous, A. et al. Modeling patient-derived glioblastoma with cerebral organoids. *Cell Rep.* **26**, 3203–3211 (2019).
23. Quaranta, V. & Linkous, A. Organoids as a systems platform for SCLC brain metastasis. *Front. Oncol.* **12**, 881989 (2022).
24. Pine, A. R. et al. Tumor microenvironment is critical for the maintenance of cellular states found in primary glioblastomas. *Cancer Discov.* **10**, 964–979 (2020).
25. Trujillo, C. A. et al. Complex oscillatory waves emerging from cortical organoids model early human brain network development. *Cell Stem Cell* **25**, 558–569 (2019).
26. Fair, S. R. et al. Electrophysiological maturation of cerebral organoids correlates with dynamic morphological and cellular development. *Stem Cell Rep.* **15**, 855–868 (2020).
27. Qu, F. et al. Crosstalk between small-cell lung cancer cells and astrocytes mimics brain development to promote brain metastasis. *Nat. Cell Biol.* **25**, 1506–1519 (2023).
28. Lee, M. H., Kong, D.-S., Seol, H. J., Nam, D.-H. & Lee, J.-I. Risk of seizure and its clinical implication in the patients with cerebral metastasis from lung cancer. *Acta Neurochir.* **155**, 1833–1837 (2013).
29. Gonzalez Castro, L. N. & Milligan, T. A. Seizures in patients with cancer. *Cancer* **126**, 1379–1389 (2020).
30. Yuen, T. I. et al. Glutamate is associated with a higher risk of seizures in patients with gliomas. *Neurology* **79**, 883–889 (2012).
31. Turrigiano, G. G., Leslie, K. R., Desai, N. S., Rutherford, L. C. & Nelson, S. B. Activity-dependent scaling of quantal amplitude in neocortical neurons. *Nature* **391**, 892–896 (1998).
32. Turrigiano, G. G. & Nelson, S. B. Hebb and homeostasis in neuronal plasticity. *Curr. Opin. Neurobiol.* **10**, 358–364 (2000).
33. Kavalali, E. T. & Monteggia, L. M. Rapid homeostatic plasticity and neuropsychiatric therapeutics. *Neuropsychopharmacol. Publ. Am. Coll. Neuropsychopharmacol.* **48**, 54–60 (2023).
34. Kavalali, E. T. & Monteggia, L. M. Targeting homeostatic synaptic plasticity for treatment of mood disorders. *Neuron* **106**, 715–726 (2020).
35. Mortazavi, A. et al. IDH-mutated gliomas promote epileptogenesis through d-2-hydroxyglutarate-dependent mTOR hyperactivation. *Neuro. Oncol.* **24**, 1423–1435 (2022).
36. Goldberg, A. R. et al. Glioma-induced alterations in excitatory neurons are reversed by mTOR inhibition. *Neuron* **113**, 858–875 (2025).
37. Johung, T. & Monje, M. Neuronal activity in the glioma microenvironment. *Curr. Opin. Neurobiol.* **47**, 156–161 (2017).
38. van Breemen, M. S. M. et al. Efficacy of anti-epileptic drugs in patients with gliomas and seizures. *J. Neurol.* **256**, 1519–1526 (2009).
39. Meldrum, B. S. & Rogawski, M. A. Molecular targets for antiepileptic drug development. *Neurother. J. Am. Soc. Exp. Neurother.* **4**, 18–61 (2007).
40. Ruggiero, A. et al. NMDA receptors regulate the firing rate set point of hippocampal circuits without altering single-cell dynamics. *Neuron* **113**, 244–259 (2025).
41. Boire, A., Brastianos, P. K., Garzia, L. & Valiente, M. Brain metastasis. *Nat. Rev. Cancer* **20**, 4–11 (2020).
42. Franchino, F., Rudà, R. & Soffietti, R. Mechanisms and therapy for cancer metastasis to the brain. *Front. Oncol.* **8**, 161 (2018).
43. Anderson, A. R. A., Weaver, A. M., Cummings, P. T. & Quaranta, V. Tumor morphology and phenotypic evolution driven by selective pressure from the microenvironment. *Cell* **127**, 905–915 (2006).
44. Barron, T. et al. GABAergic neuron-to-glioma synapses in diffuse midline gliomas. *Nature* **639**, 1060–1068 (2025).
45. Peinado, P. et al. Intrinsic electrical activity drives small-cell lung cancer progression. *Nature* **639**, 765–775 (2025).
46. Dobrunz, L. E. & Stevens, C. F. Heterogeneity of release probability, facilitation, and depletion at central synapses. *Neuron* **18**, 995–1008 (1997).
47. Guzikowski, N. J. & Kavalali, E. T. Nano-organization of spontaneous GABAergic transmission directs its autonomous function in neuronal signaling. *Cell Rep.* **40**, 111172 (2022).
48. Horvath, P. M., Piazza, M. K., Monteggia, L. M. & Kavalali, E. T. Spontaneous and evoked neurotransmission are partially segregated at inhibitory synapses. *Elife* **9**, 52852 (2020).
49. Jackman, S. L. & Regehr, W. G. The mechanisms and functions of synaptic facilitation. *Neuron* **94**, 447–464 (2017).
50. Tetzlaff, S. K. et al. Characterizing and targeting glioblastoma neuron-tumor networks with retrograde tracing. *Cell* (2024) <https://doi.org/10.1016/j.cell.2024.11.002>.
51. Gay, C. M. et al. Patterns of transcription factor programs and immune pathway activation define four major subtypes of SCLC with distinct therapeutic vulnerabilities. *Cancer Cell* **39**, 346–360 (2021).
52. Venkatesh, H. S. et al. Targeting neuronal activity-regulated neuroligin-3 dependency in high-grade glioma. *Nature* **549**, 533–537 (2017).
53. Venkatesh, H. S. et al. Neuronal activity promotes glioma growth through neuroligin-3 secretion. *Cell* **161**, 803–816 (2015).
54. Campbell, S. L., Buckingham, S. C. & Sontheimer, H. Human glioma cells induce hyperexcitability in cortical networks. *Epilepsia* **53**, 1360–1370 (2012).
55. Buckingham, S. C. et al. Glutamate release by primary brain tumors induces epileptic activity. *Nat. Med.* **17**, 1269–1274 (2011).
56. Pallud, J. et al. Cortical GABAergic excitation contributes to epileptic activities around human glioma. *Sci. Transl. Med.* **6**, 244ra89 (2014).
57. Yu, K. et al. PIK3CA variants selectively initiate brain hyperactivity during gliomagenesis. *Nature* **578**, 166–171 (2020).
58. Frere, S. & Slutsky, I. Alzheimer's disease: from firing instability to homeostasis network collapse. *Neuron* **97**, 32–58 (2018).
59. Styr, B. & Slutsky, I. Imbalance between firing homeostasis and synaptic plasticity drives early-phase Alzheimer's disease. *Nat. Neurosci.* **21**, 463–473 (2018).

60. Huang, D. et al. Cancer-cell-derived GABA promotes β -catenin-mediated tumour growth and immunosuppression. *Nat. Cell Biol.* **24**, 230–241 (2022).
61. Takehara, A. et al. Gamma-aminobutyric acid (GABA) stimulates pancreatic cancer growth through overexpressing GABAA receptor π subunit. *Cancer Res.* **67**, 9704–9712 (2007).
62. Liu, Q. et al. Anesthetic propofol promotes tumor metastasis in lungs via GABA(A) R-dependent TRIM21 modulation of SRC expression. *Adv. Sci.* **8**, e2102079 (2021).
63. Ippolito, J. E. et al. Linkage between cellular communications, energy utilization, and proliferation in metastatic neuroendocrine cancers. *Proc. Natl. Acad. Sci. USA* **103**, 12505–12510 (2006).
64. Barny, L. A. et al. Proteostasis and unfolded protein response dynamics in human neuron and mouse glia co-culture reveal cell-specific aging responses. *bioRxiv Prepr. Serv. Biol.* (2025) <https://doi.org/10.1101/2025.08.11.669714>.
65. Linkous, A. & Fine, H. A. Generating Patient-Derived Gliomas within Cerebral Organoids. *STAR Protoc.* **1**, (2020).
66. Clark, I. C. et al. Microfluidics-free single-cell genomics with templated emulsification. *Nat. Biotechnol.* (2023) <https://doi.org/10.1038/s41587-023-01685-z>.
67. Soneson, C. & Robinson, M. D. Bias, robustness and scalability in single-cell differential expression analysis. *Nat. Methods* **15**, 255–261 (2018).

Acknowledgements

We thank all members of the Kavalali and Monteggia lab for constructive comments and feedback. We thank Dr. Zhenzhong Ma for productive recommendations and fruitful conversations on this project as well as Dr. Rick Sando and Dr. Krassimira Garbett for assistance in confocal microscopy. The cartoon figure captions in this study were generated using Biorender.com. This work was supported by National Institutes of Health grant 5R01MH066198-21 to E.T.K. and 5U54CA217450-05 to V.Q.

Author contributions

Conceptualization: A.H., E.T.K., and A.L. Methodology: A.H., B.U., A.L., G.V.I., and T.O. Investigation: A.H., B.U., A.L., G.V.I., and T.O. Visualization: A.H. and E.T.K. Funding acquisition: E.T.K. and V.Q. Project administration: A.H., L.M.M., and E.T.K. Supervision: E.T.K., L.M.M., and V.Q. Writing – original draft: A.H. Writing – review & editing: A.H., E.T.K., B.U., A.L., V.Q., and G.V.I.

Competing interests

The authors declare no competing interests.

Additional information

Supplementary information The online version contains supplementary material available at <https://doi.org/10.1038/s42003-025-09006-7>.

Correspondence and requests for materials should be addressed to Ege T. Kavalali.

Peer review information The manuscript was considered suitable for publication without further review at *Communications Biology*. Primary Handling Editor: Johannes Stortz.

Reprints and permissions information is available at <http://www.nature.com/reprints>

Publisher's note Springer Nature remains neutral with regard to jurisdictional claims in published maps and institutional affiliations.

Open Access This article is licensed under a Creative Commons Attribution-NonCommercial-NoDerivatives 4.0 International License, which permits any non-commercial use, sharing, distribution and reproduction in any medium or format, as long as you give appropriate credit to the original author(s) and the source, provide a link to the Creative Commons licence, and indicate if you modified the licensed material. You do not have permission under this licence to share adapted material derived from this article or parts of it. The images or other third party material in this article are included in the article's Creative Commons licence, unless indicated otherwise in a credit line to the material. If material is not included in the article's Creative Commons licence and your intended use is not permitted by statutory regulation or exceeds the permitted use, you will need to obtain permission directly from the copyright holder. To view a copy of this licence, visit <http://creativecommons.org/licenses/by-nc-nd/4.0/>.

© The Author(s) 2025